

Imprints of Sagittarius accretion event: Young O-rich stars and discontinuous chemical evolution in Milky Way disc

Tiancheng Sun^{1,2}, Shaolan Bi^{1,2*}, Xunzhou Chen^{3*}, Yuqin Chen^{4,1,5}, Chao Liu^{4,1,5}, Xianfei Zhang^{1,2}, Tanda Li^{1,2}, Yaguang Li⁶, Yaqian Wu⁴, Zhishuai Ge⁷, Lifei Ye^{1,2}

^{1*}Institute for Frontiers in Astronomy and Astrophysics, Beijing Normal University, Beijing, 102206, China.

²Department of Astronomy, Beijing Normal University, Beijing, 100875, China.

³Research Center for Intelligent Computing Platforms, Zhejiang Laboratory, Hangzhou, 311100, China.

⁴Key Lab of Space Astronomy and Technology, National Astronomical Observatories, Beijing, 100101, China.

⁵University of Chinese Academy of Sciences, Beijing, 100049, China.

⁶Institute for Astronomy, University of Hawai'i, 2680 Woodlawn Drive, Honolulu, HI 96822, USA.

⁷Beijing Planetarium, Beijing Academy of Science and Technology, Beijing, 100044, China.

*Corresponding author(s). E-mail(s): bisl@bnu.edu.cn; cxz@zhejianglab.com;

Abstract

The Milky Way has undergone significant transformations in its early history, characterised by violent mergers and the accretion of satellite galaxies. Among these events, the infall of the satellite galaxy Gaia-Enceladus/Sausage is recognised as the last major merger event, fundamentally altering the evolution of the Milky Way and shaping its chemo-dynamical structure. However, recent observational evidence suggests that the Milky Way remains undergone notable events of star formation in the past 4 Gyr, which is thought to be triggered by the perturbations from Sagittarius dwarf galaxy (Sgr). Here we report chemical signatures of the Sgr accretion event in the past 4 Gyr, using the [Fe/H] and [O/Fe] ratios in the thin disc, which is reported for the first time. It reveals that the previously discovered V-shape structure of age-[Fe/H] relation varies across different Galactic locations and has rich substructures. Interestingly, we discover a discontinuous structure at $z_{\max} < 0.3$ kpc, interrupted by a recent burst of star formation from 4 Gyr to 2 Gyr ago. In this episode, we find a significant rise in oxygen abundance leading to a distinct [O/Fe] gradient, contributing to the formation of young O-rich stars. Combined with the simulated star formation history and chemical abundance of Sgr, we suggest that the Sgr is an important actor in the discontinuous chemical evolution of the Milky Way disc.

Recent findings, utilising data from the European Space Agency (ESA) Gaia mission [2, 3] and the Galactic Archaeology with HERMES (GALAH)

[4–6] survey, have revealed an enhanced star formation rate during the past 2–4 Gyr [7–10]. This phenomenon is believed to be associated with the

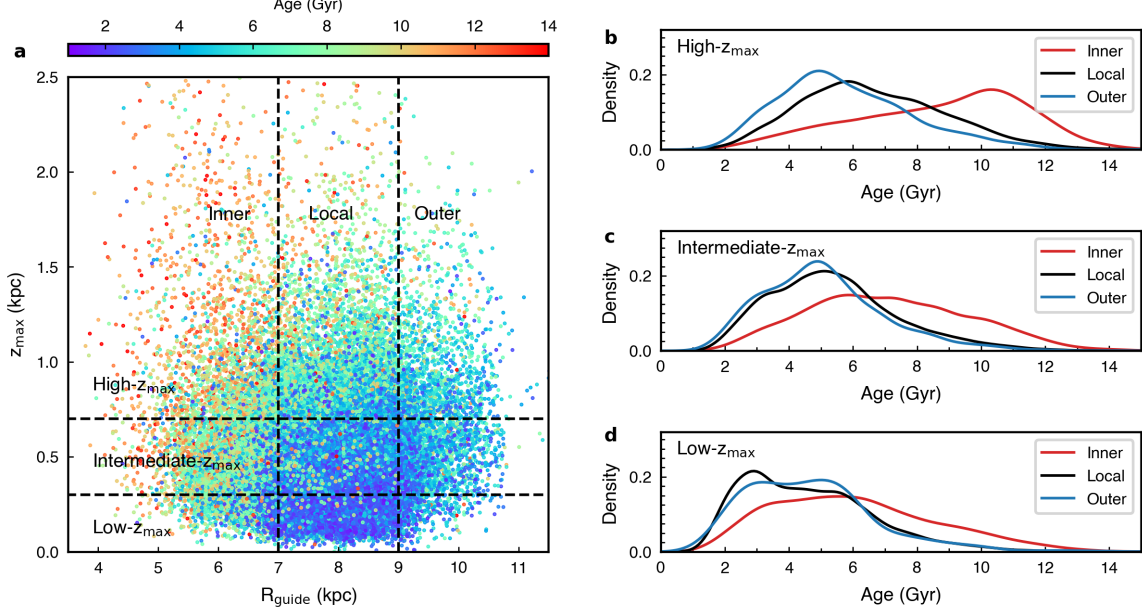


Fig. 1 The age distributions of our star sample. **a**, $R_{\text{guide}}-z_{\text{max}}$ distributions of sample stars, colour-coded by stellar ages. The vertical dashed lines in the top panel indicate the division into three R_{guide} bins (inner, local, and outer) at $R_{\text{guide}} = 7$ and 9 kpc. The horizontal dashed line indicates the division of each R mean bin into three z_{max} bins (high- z_{max} , intermediate- z_{max} , low- z_{max}) at $z_{\text{max}} = 0.3$ and 0.7 kpc. **b**, The age distributions (based on the kernel density estimates) of spatially selected subsamples (inner, local, and outer) in high- z_{max} region. **c**, The age distributions of spatially selected subsamples (inner, local, and outer) in intermediate- z_{max} region. **d**, The age distributions of spatially selected subsamples (inner, local, and outer) in low- z_{max} region.

pericentre passages of the Sagittarius dwarf galaxy (Sgr) [11–13]. Here we employ an oxygen-enhanced stellar model [10] to reliably determine the ages of main-sequence turnoff and subgiant stars from the Third Data Release of GALAH [6] (GALAH DR3) focusing primarily of unveiling the impact on star formation history by recent accretion events. Our approach utilises a Bayesian methodology [14], incorporating spectroscopic chemical abundances, specifically $[\text{Fe}/\text{H}]$, $[\alpha/\text{Fe}]$ (where α refers to Mg, Si, Ca, and Ti), and $[\text{O}/\text{Fe}]$, alongside T_{eff} and luminosity [15]. The application of the oxygen-enhanced stellar model together with precise luminosity from Gaia and reliable abundance measurements from GALAH enable us to ascertain the age-abundance relations and track the evolution of the abundance gradient in the Galactic disc with unparalleled precision.

1 Age–abundance distribution of the Milky Way disc

Fig. 1 shows the R_{guide} versus z_{max} diagram and the derived age distributions of spatially selected

subsamples. It is found that there are clear differences in age distributions (Fig. 1b,c,d) with R_{guide} (guiding radius) and z_{max} (maximum vertical distance from the disc plane). The mean ages of disc components (inner, local, and outer disc) at low- z_{max} region are younger on average than the intermediate- z_{max} and high- z_{max} regions with most stars younger than 8 Gyr. It is noted that there is a young peak at ~ 3 Gyr in the age distributions of local and outer disc at low- z_{max} region (Fig. 1d), which is more prominent for local disc. This bump is also seen in the intermediate- z_{max} region (Fig. 1c) but disappears in the high- z_{max} region (Fig. 1b). In addition, most of subsamples have an age peak at 5–6 Gyr, except for the inner disc at high- z_{max} region, which has an age peak at ~ 10.5 Gyr. The young peak of age distributions indicate that there is a recent burst of star formation in the local and outer disc ~ 3 Gyr ago, while the intermediate-aged peak at 5–6 Gyr is thought to be the star formation triggered by the first pericentric passages of Sgr (~ 5.5 Gyr ago) [12].

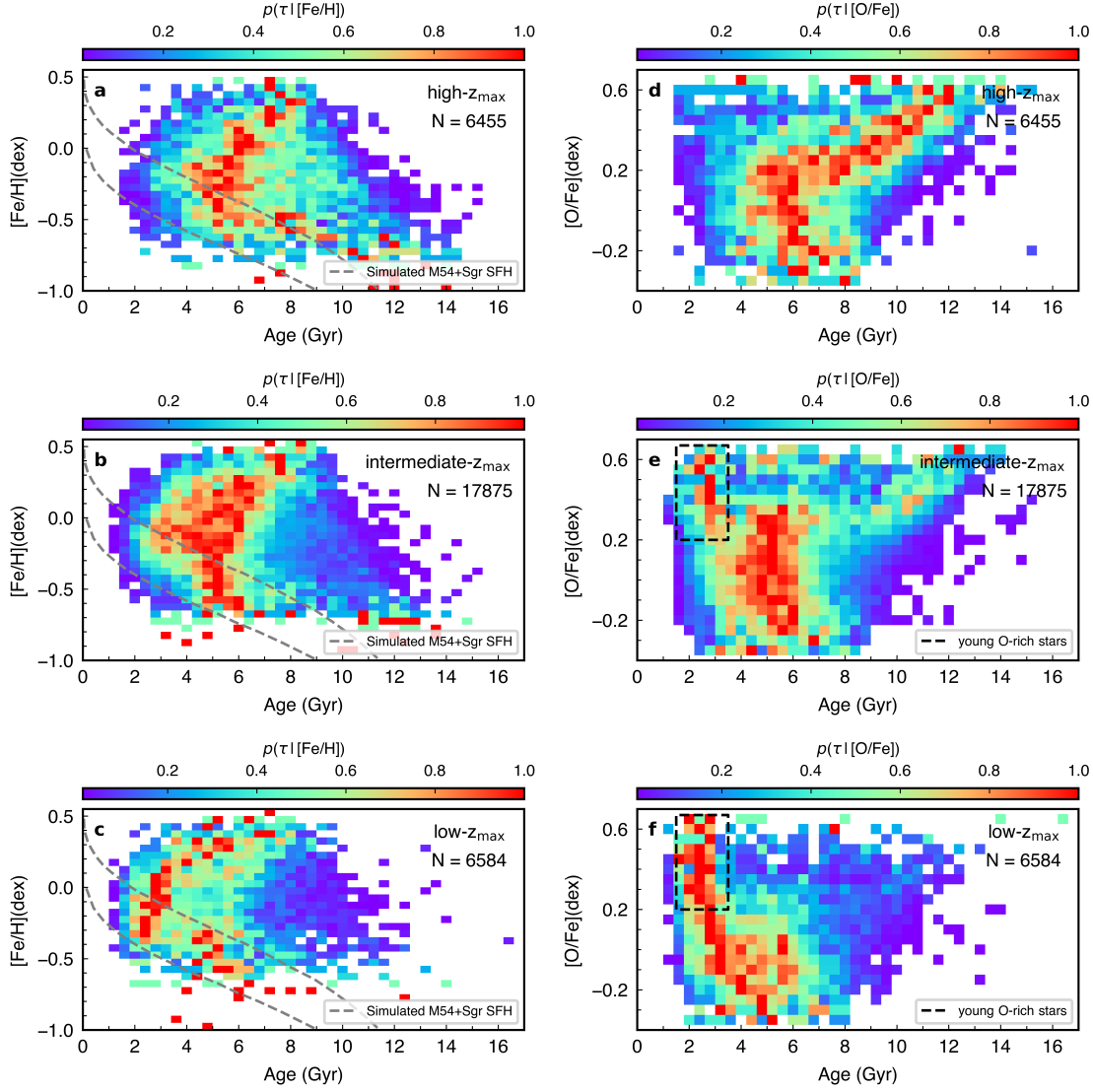


Fig. 2 Stellar age–abundance relation of local disc revealed by our star sample. **a, b, c**, Age–[Fe/H] distributions of the local disc stars at high- z_{\max} , intermediate- z_{\max} , and low- z_{\max} regions, according to the division in Fig.1a. The gray dashed lines represent the simulated M54 + Sgr star formation history (SFH) from literature [1]. **d, e, f**, Age–[O/Fe] distributions of the local disc stars at high- z_{\max} , intermediate- z_{\max} , and low- z_{\max} regions. The black dashed lines indicate the young O-rich stars. **a**, Probability distribution of stellar age $p(\tau|[Fe/H])$, normalised to the peak value for each [Fe/H], for local disc stars at high- z_{\max} region. **d**, Probability distribution of stellar age $p(\tau|[O/Fe])$, normalised to the peak value for each [Fe/H], for local disc stars at high- z_{\max} region. **b, c**, Similar to **a** but for local disc stars at intermediate- z_{\max} and low- z_{\max} regions. The black dashed boxes indicate the overdensities in the $p(\tau|[Fe/H])$ distribution of local disc. **e, f**, Similar to **d** but for local disc stars at intermediate- z_{\max} and low- z_{\max} regions. The blue dashed boxes show the young oxygen-enhanced populations in the local disc.

The distributions of nine spatially selected subsamples in age–[Fe/H] and age–[O/Fe] planes are presented in Fig.A2 and Fig.A3. Fig.A3 shows that there is a increasing trend of [O/Fe] with decreasing age in young (age < 3 Gyr) and intermediate (4 Gyr < age < 6 Gyr) populations.

The oxygen-enhancement of young populations is most prominent in local age–[O/Fe] relations (Fig.A3e,h), which correspond to the overdensities in local age–[Fe/H] relations (Fig.A2e,h).

To better investigate the elemental enrichment history of the local disc, we employ a normalization procedure for the distribution $p(\tau, [\text{Fe}/\text{H}])$ of local disc stars to obtain $p(\tau|[\text{Fe}/\text{H}])$, the age distribution at a specified $[\text{Fe}/\text{H}]$. As presented in Fig. 2a,b,c, the resulting $p(\tau|[\text{Fe}/\text{H}])$ distribution of local disc exhibit a gradual variation with z_{max} , from a so called "V-shape" [10, 16] (at age < 8 Gyr) at high- z_{max} and intermediate- z_{max} regions to a discontinuous structure at low- z_{max} region. This feature implies that the previously discovered V-shape structure [10, 16] depends on the location in the Milky Way disc. For the local disc at high- z_{max} region, the distribution of $p(\tau|[\text{Fe}/\text{H}])$ exhibits a V-shape; at intermediate- z_{max} region, this V-shape is more pronounced and an overdensity with near-solar metallicity appears at 2-4 Gyr. In the low- z_{max} region, the V-shape structure becomes discontinuous, and this discontinuity corresponds to a decrease (Fig. 2c) in iron abundance and a sharp increase (Fig. 2f) in oxygen abundance, suggesting that a fresh gas interrupted the secular evolution of the Milky Way disc [17]. To our knowledge, this feature has not been seen before.

The increasing trend of oxygen abundance from 4 Gyr to 2 Gyr (Fig. 2f) is a strong evidence of enhanced star formation in the local disc, as the oxygen is mainly produced by hydrostatic burning in massive stars and subsequently dispersed to the interstellar medium in SNeII (Type II supernovae) explosions [18, 19]. This increasing trend is also visible in Fig. 2e and disappears in Fig. 2d, contributing to the formation of young O-rich stellar population. On the other hand, it is noted that the age- $[\text{Fe}/\text{H}]$ relations observed in Fig. 2a,b,c are in consistent with the simulated star formation history (SFH) of the M54+Sgr system based on Hubble Space Telescope photometry [20], which find an intermediate-aged star formation epochs from 6 Gyr at $[\text{Fe}/\text{H}] = -0.6$ to 4 Gyr at $[\text{Fe}/\text{H}] = -0.4$, plus a prominent, ~ 2.3 Gyr old Sgr population of near-solar abundance [1]. The metal-poor branch with $[\text{Fe}/\text{H}] \lesssim -0.2$ in Fig. 2a,b,c, and the overdensity of near-solar $[\text{Fe}/\text{H}]$ in Fig. 2b,c, demonstrate a similarity (falls between two simulated SFH) with the SFH of M54+Sgr, and reinforce the idea of Sgr being the main actor behind conspicuous enhancements of star formation in the Milky Way during the past 6 Gyr.

2 Temporal evolution of radial abundance gradient

The oxygen enrichment and metallicity depletion ($[\text{Fe}/\text{H}]$) strongly suggest that Sgr have influenced the evolution of our Galaxy in the past few billion years. Previous studies on the Gaia-Enceladus/Sausage (GSE) have highlighted the significant role of massive mergers in shaping the Galactic disc and altering the radial metallicity gradient in the past 8-11 Gyr [21–24]. To study the influence of minor merger events (Sgr accretion) on the radial metallicity gradient during the later stages of Galaxy evolution. We examine the temporal evolution of the radial abundance gradient in the Milky Way disc by utilising precise stellar ages from our stellar models.

Fig. 3 presents the radial profiles of $[\text{Fe}/\text{H}]$ and $[\text{O}/\text{Fe}]$ for disc stars divided into eight age bins. Notably, the $[\text{Fe}/\text{H}]$ profile undergoes a substantial transformation, transitioning from a positive gradient at 12-14 Gyr to a negative gradient at 6-8 Gyr, and subsequently maintaining a relatively steady negative gradient until 3 Gyr ago. A significant departure from this stable gradient occurs at 1-3 Gyr, as the $[\text{Fe}/\text{H}]$ profile becomes flatter compared to the 3-8 Gyr period and resembles the gradient observed at 8-10 Gyr. This behaviour indicates that the recent star formation burst has a global effect on the evolution of thin disc, flattening the radial metallicity gradient.

The radial $[\text{Fe}/\text{H}]$ profile at 10-12 Gyr exhibits a break at ~ 7.5 kpc, featuring a positive slope within the break radius and a negative slope beyond it. Similarly, the radial $[\text{Fe}/\text{H}]$ profile at 8-10 Gyr ago shows a break at ~ 6.5 kpc, with a flat slope within the break radius and a negative slope beyond it. These break radii is consistent with the break radius observed in the radial profile of integrated stellar metallicity using red giant branch stars [25]. Moreover, leveraging the high precision in age, we identify that these breaks primarily occur within the 8-12 Gyr, which was not apparent in the metallicity profiles of mono-age populations in previous studies [25].

The radial $[\text{O}/\text{Fe}]$ profile exhibits a transition from a negative gradient at 12-14 Gyr to a positive gradient at 6-8 Gyr, followed by a relatively stable positive gradient until 3 Gyr ago. Similar to the radial $[\text{Fe}/\text{H}]$ profile, a significant departure

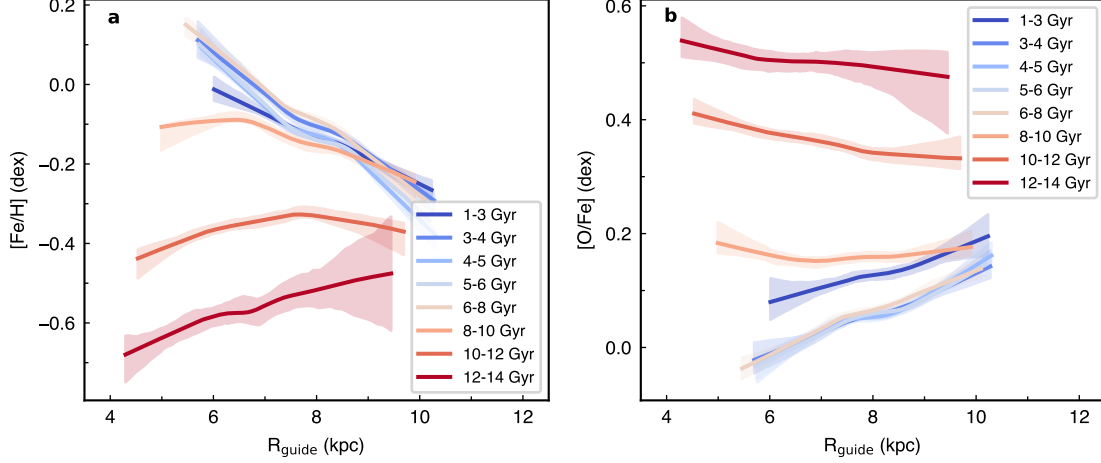


Fig. 3 Radial abundance profile in bins of age. **a**, Radial [Fe/H] profile in bins of age, each line represent the local nonparametric regression fitting to the distribution of sample stars in this age bins. The shaded regions indicate the 95% confidence interval around the fitting result by performing bootstrap resampling. **b**, Similar to **a** but for radial [O/Fe] profile in bins of age.

from this stable radial [O/Fe] profile occurs at 1-3 Gyr, with a flatter gradient compared to the 3-8 Gyr period. Overall, the flattened radial [Fe/H] and radial [O/Fe] profiles imply that an accretion event has diluted the metallicity of the disc and led to an enhancement of oxygen abundance.

The Bayesian linear fitting [26] are performed to the radial [Fe/H]/[O/Fe] profiles in 1 Gyr age bins (Fig. 4) to present the distinctive characteristics of them. These analyses are restricted to a thinner slice of the Galactic disc ($|Z_{\text{Gal}}| < 0.3$ kpc and $5 \text{ kpc} < R_{\text{Gal}} < 11 \text{ kpc}$), as the young peak of age distribution is mainly observed in the low z_{max} disc. Fig. 4a shows a rise in [Fe/H] and [O/Fe] gradient between 4 and 2 Gyr ago, which corresponds to the enhanced star formation episode triggered by second passages of the Sgr galaxy [11, 12]. During this episode, an enhanced dispersion about radial [O/Fe] gradient with respect to the trend appears between 6 and 4 Gyr ago, indicating that an accretion event influencing the overall evolution of the thin disc. However, there is no obvious feature of enhanced dispersion about radial [Fe/H] gradient. The difference between the dispersion of [Fe/H] and [O/Fe] suggests that this accretion event was a minor merger event and thus introduced a small dispersion of [Fe/H] (the overdensity in Fig. 2e). Furthermore, at the early stage (8-11 Gyr) of Milky Way, there is a quick steepening in [Fe/H] and [O/Fe] gradient, linked to the effect of the GSE merger event [22, 24], slighter later (by

~ 0.5 Gyr, see Fig. A4) than the epoch based on the LAMOST [27, 28] and APOGEE [29, 30] data [22, 23]. These discrepancies could be attributed to different methods of age determination. Compared to the results from α EM model (e.g., Yonsei-Yale stellar isochrones used in LAMOST data), the ages of thick disc stars are significantly younger based on the oxygen-enhanced stellar models [10].

3 Evidence for the pericentric passage of Sagittarius

All results presented in this study strongly suggest the occurrence of a recent star formation burst in the Milky Way disc within the epoch of the recent passages of the Sgr (2-3 Gyr ago) [1, 11, 31], altering the radial abundance profiles. Previous investigations toward the chemical compositions of Sgr stars have found that the stars with $[\text{Fe}/\text{H}] \geq -0.5$ exhibit notable deficiencies in $[\text{Mg}/\text{Fe}]$ compared to the Milky Way disc [32-38]. Fig. 5 shows the abundance-age relations (age-[Mg/Fe] and age-[Ca/Fe]) of local low z_{max} disc. Intriguingly, there is a notable declining trend of [Mg/Fe] with age from 4 Gyr to ~ 2 Gyr, indicating that the newly formed disc stars are Mg-poor. The magnesium and oxygen are believed to be primarily synthesised during the hydrostatic burning phase of massive stars and subsequently ejected via the SNeII explosions [18, 19]. Despite some works

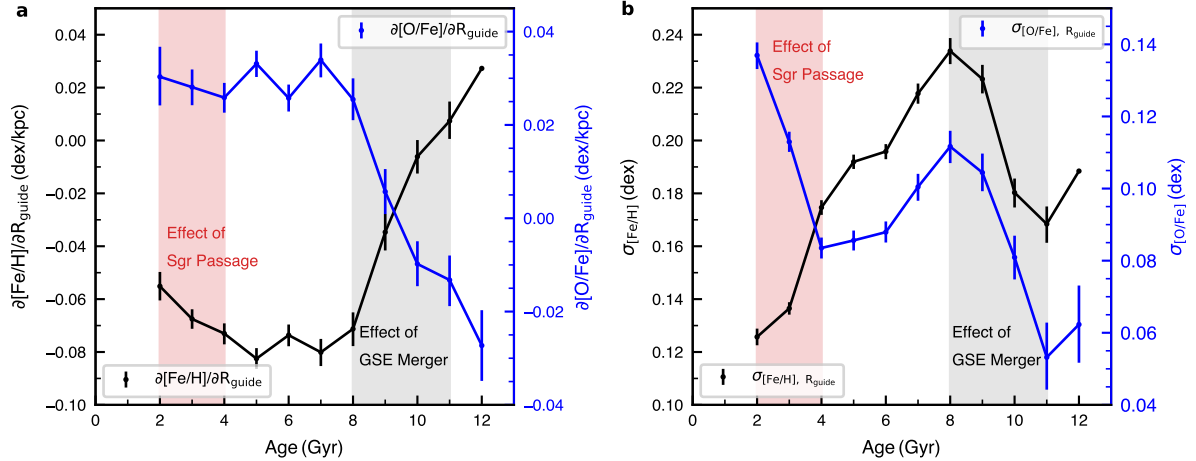


Fig. 4 Age dependence of the radial abundance gradient and the corresponding abundance dispersion around the gradient. **a**, Age dependence of the radial [Fe/H] (black) gradient and radial [O/Fe] (blue) gradient, in terms of guiding-centre radii (R_{guide}). Each point was obtained by 3-parameter (slope, intercept, and dispersion) Bayesian fits to the [Fe/H]/[O/Fe]- R_{guide} distribution, using only data in the respective age bin, restricted to $|Z_{\text{Gal}}| < 0.3$ kpc and $5 \text{ kpc} < R_{\text{Gal}} < 11 \text{ kpc}$. The grey-shaded area marks the age interval in which we expect to see signatures from the Gaia Sausage/Enceladus (GSE) merger event, while the red-shaded area marks the age interval for the effect of (Sagittarius dwarf galaxy) passage. **b**, Age dependence of the [Fe/H] (black) and [O/Fe] (blue) dispersion around the radial [Fe/H]/[O/Fe] gradient (**a**), in terms of R_{guide} .

[39, 40] have shown that Mg might also be partially released into the interstellar medium by SNe Ia (type Ia supernovae), this can not explain the opposite trend of O and Mg versus age from 4 Gyr to 2 Gyr ago. In addition, similar to the trend of oxygen abundance, an increasing trend of [Ca/Fe] from 4 Gyr to 2 Gyr is observed. The peculiar behaviours of magnesium and oxygen abundances could be attributed to gas dilution from Sgr, with gas stripping estimated to be 30-50 percent complete at its disc crossing approximately 2.7 Gyr ago [11].

Although Sgr is not the only satellite of the Milky Way that might be affecting our Galaxy presently, it exhibits the closest resemblance in chemical signature to the infalling gas responsible for the observed deficiencies in magnesium abundance. A comparative analysis [38] of the chemical compositions of various Milky Way dwarf satellite galaxies, based on APOGEE data [29, 30], has shown that among the ten known Milky Way dwarf satellites, Sgr stands out as the only satellite possessing near-solar metallicity ([Fe/H] ~ -0.1) and a deficit in [Mg/Fe] ~ -0.2 . In contrast, another satellite within a similar metallicity range, the Large Magellanic Cloud (LMC), does

not exhibit a distinct depletion in [Mg/Fe], with [Mg/Fe] ~ -0.05 at the metal-rich end [38].

We utilise data from the APOGEE DR17 [30] to compare the chemical composition of Sgr stars [36] with the young population (1-4 Gyr) in our sample (see Fig.A5 and Fig.A6). The results clearly demonstrate that between 3-4 Gyr, the [Mg/Fe] ratios of metal-rich Sgr stars are ~ -0.2 dex at [Fe/H] = -0.2 , which is lower than that of disc stars in the Milky Way at the same [Fe/H] value. Conversely, the [Ca/Fe] ratios of metal-rich Sgr stars are ~ 0 dex, slightly higher (by around 0.1 dex) than those of Ca-poor disc stars in the Milky Way at fixed [Fe/H]. A similar pattern is observed for O, which is more pronounced than Ca. In the later epoch of 1-3 Gyr, there is an increased presence of Mg-poor stars in the Milky Way disc, as also shown in Fig.5c. Meanwhile, these stars exhibit enhancement in O and Ca. The comparison of Sgr stars and Milky Way disc stars in [Fe/H]-[X/Fe] planes indicates that the infall gas from Sgr influences subsequent star formation in the Milky Way disc.

We suggest that the behaviour of α -elements during the 1-3 Gyr epoch depends on two factors: 1. the chemical abundance of Sgr relative to

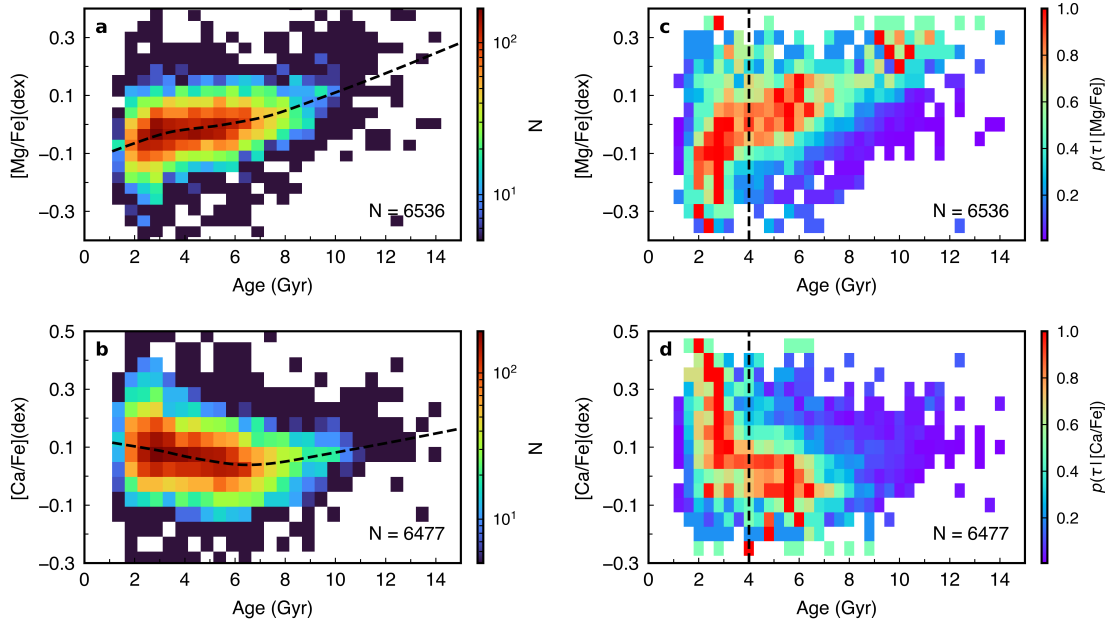


Fig. 5 **Stellar age–abundance relation of local disc at low- z_{\max} region, revealed by our star sample.** **a, b,** Age- $[\text{Mg}/\text{Fe}]$ and age- $[\text{Ca}/\text{Fe}]$ distributions for local disc stars at low- z_{\max} region, colour-coded by the stellar number density, N . The black dashed lines represent the fitting result by local nonparametric regression. **c, d,** Probability distribution of stellar age $p(\tau)|[\text{Mg}/\text{Fe}]/p(\tau)|[\text{Ca}/\text{Fe}]$, normalised to the peak value for $[\text{Mg}/\text{Fe}]/[\text{Ca}/\text{Fe}]$, similar to Fig. 2, but for other α -elements (Mg and Ca). The black dashed lines represent the location at age = 4 Gyr.

the Milky Way disc, specifically whether each α -element is deficient or enhanced compared to disc stars; 2. the recent star formation in the Galactic disc triggered by Sgr, which produces a substantial amount of α -elements and leads to their enrichment in newly formed stars. In the two factors, Mg exhibits distinct behaviours. They are significantly deficient in Sgr relative to the disc stars in the Milky Way, explaining the observed decreasing trend in Fig. 5c. In contrast, O and Ca show a monotonous increasing trend.

In this work, we find that the V-shape structure of age- $[\text{Fe}/\text{H}]$ relation depends on the location in the Galactic disc. This structure becomes discontinuous at $z_{\max} < 0.3$ kpc, interrupted by a decrease in metallicity ($[\text{Fe}/\text{H}]$) and a significant increase in oxygen abundance from 4 Gyr to 2 Gyr ago, which is reported for the first time. The timing and chemical signature of this event is consistent with the simulated chemical evolution of Sgr. In addition, this event gives rise to distinct radial profiles of $[\text{Fe}/\text{H}]/[\text{O}/\text{Fe}]$ compared to earlier stage. The dispersion around the radial $[\text{O}/\text{Fe}]$ gradient exhibits a remarkable increase as age decreases within the same epoch (2-4 Gyr). These

findings indicate that Sagittarius dwarf galaxy can trigger star formation burst across the disc, reshaping the chemical evolution of the Milky Way disc, contributing to the formation of young O-rich stars. Moreover, this study imposes important constraints on the chemical evolution models of the Milky Way, highlighting the need for further analysis to unravel the underlying physical mechanisms responsible for the global effects of star formation events induced by interactions with low-mass satellites such as Sgr.

Acknowledgments. The authors acknowledge Joss Bland-Hawthorn and Sven Buder for helpful discussions. The authors thank Thomas G. Bisbas for improving the presentation of manuscript. This work used the data from the GALAH survey, which is based on observations made at the Anglo Australian Telescope, under programs A/2013B/13, A/2014A/25, A/2015A/19, A/2017A/18, and 2020B/23. This work has made use of data from the European Space Agency (ESA) mission Gaia (<https://www.cosmos.esa.int/gaia>), processed by the Gaia Data Processing and Analysis Consortium (DPAC, <https://www.cosmos.esa.int/web/>

[gaia/dpac/consortium](https://gaia.dpac.consortium)). Funding for the DPAC has been provided by national institutions, in particular the institutions participating in the Gaia Multilateral Agreement. This work has made use of data and analysis code from the Anders et al. 2023 (https://github.com/fjaellet/xgboost_chem_ages) [23]. This work is supported by the Joint Research Fund in Astronomy (U2031203) under cooperative agreement between the National Natural Science Foundation of China (NSFC) and Chinese Academy of Sciences (CAS), the NSFC grants (12090040, 12090042, 12373020), and the National Key R&D Program of China No. 2019YFA0405503, 2023YFE0107800. This work is partially supported by the Scholar Program of Beijing Academy of Science and Technology (DZ:BS202002).

Declarations

- Data availability
The relevant datasets are available from the corresponding author upon reasonable request.
- Code availability
No new codes are developed in this paper.

Appendix A Method

A.1 GALAH data and sample selection

This work is based on the data from the Third Data Release of the Galactic Archaeology with HERMES survey (GALAH DR3) [6]. GALAH DR3 [6] provides stellar parameters (T_{eff} , $\log g$, $[\text{Fe}/\text{H}]$, V_{mic} , V_{broad} , V_{rad}) and up to 30 elemental abundances for 588,571 stars, derived from optical spectra at a typical resolution of $R \sim 28,000$. The $[\text{Fe}/\text{H}]$, $[\text{O}/\text{Fe}]$, $[\text{Mg}/\text{Fe}]$, $[\text{Si}/\text{Fe}]$, $[\text{Ca}/\text{Fe}]$ ratios from GALAH DR3 was calculated based on a non-LTE method (LTE: local thermodynamic equilibrium) [41]. The data set used in this work is mainly from Sun et al. 2023 [10]. We extended this sample [10] to cover a T_{eff} range of 4800–7000 K, and a $\log g$ range of 3.2–4.1. Following the recommendations in GALAH DR3, we apply stringent selection criteria to ensure reliable stellar parameters, including iron, α -elements, and oxygen abundances ($\text{flag_sp} = 0$, $\text{flag_fe_h} = 0$, $\text{flag_alpha_fe} = 0$, and $\text{flag_o_fe} = 0$), requiring

an $\text{SNR} > 30$, a $\text{chi2_sp} < 4$ (Chi2 value of stellar parameter fitting), and a quality flag = 0. Binary systems identified by Traven et al. 2020 [42] and Yu et al. 2023 [15] are excluded. Additionally, we apply a single cut based on the Gaia DR3 parameters by selecting stars with a Gaia re-normalised unit weight error (RUWE) of less than 1.2. Giant stars are excluded by applying the absolute magnitude cut [9]:

$$M_{K_s} = m_{K_s} - A_{K_s} - 5 \log_{10}[(100 \text{ mas})/\varpi] > 8.5 - T_{\text{eff}}/(700 \text{ K}) \quad (\text{A1})$$

The extinction values A_{K_s} and the 2MASS m_{K_s} magnitudes [43] used here are taken from the GALAH catalogue. In addition, we remove all stars with M_K brighter than 0.5 mag to avoid contamination from He-burning horizontal branch stars [16]. To focus on disc stars, we select samples with $[\text{Fe}/\text{H}] > -1$, eccentricity < 0.5 , and $|Z_{\text{Gal}}| < 1$ kpc, and removed the halo stars mentioned in Sun et al. 2023 [10]. To ensure the accuracy of our results, we remove stars with a relative age uncertainty greater than 30 per cent. Additionally, we exclude 2 stars with significant model systematic bias, whose inferred ages are 2σ larger than the age of the Universe (13.8 Gyr) [44]. After applying these cuts, our final sample consisted of 45,186 MSTO and subgiant stars, with a median relative age uncertainty of 9.8 per cent across the age range of 1–13.8 Gyr, as shown in Fig.A1. We obtain the luminosities of sample stars by cross-match them with the catalogue from Yu et al. 2023 [15], which provides the luminosity of 1.5 million stars using astrometric data from GAIA DR3 [45] and improved interstellar extinction measurements.

We utilised the orbital parameters (eccentricity) and velocities (U , V , W , and V_Z) from the GALAH DR3 value-added catalogue (VAC) [6]. These values are calculated from the astrometry provided by Gaia EDR3 and radial velocities determined from the GALAH spectra [46]. The orbital parameters in this catalogue are calculated using the Python package *Galpy* [47], with the details of assumed Milky Way potential and solar kinematic parameters presented in Buder et al. 2021 [6]. We calculated the guiding radii R_{guide} with the same input parameters (distance, ra , dec ,

radial velocity, pmra, pmdec), Milky Way potential, and solar kinematic parameters presented in Buder et al. 2021 [6].

A.2 Age estimation based on Oxygen-enhanced stellar models

We use oxygen-enhanced stellar evolution models to estimate ages of sample stars. The oxygen-enhanced stellar models use an individual O enhancement factor, thereby allowing the O abundance to be specified independently (see Sun et al. 2023 [10] for details). The other α -elements (i.e., Ne, Mg, Si, S, Ca, and Ti) are maintained with the same enhancement factor. Neglecting to account for the independent enhancement of oxygen abundance in age determination would result in significant age biases, which would obscure the age-[O/Fe] relation [48]. Therefore, the oxygen-enhanced models could accurately characterising the age-[O/Fe] relation of sample stars.

The ages of the MTSO and subgiant sample stars are determined by matching the Gaia Luminosity [15], the GALAH spectroscopic stellar parameters T_{eff} , [Fe/H], [α /Fe], and [O/Fe], with the Oxygen-enhanced stellar models [10] using a Bayesian approach [14] (Sun et al. 2023 [10], for more details).

Since our age estimates are independent from kinematics of sample stars. As an test for our age estimation, we show the age-velocity relation (AVR) of sample stars in Fig.A7. Fig.A7a shows the AVR of our sample in local region, with a Galactocentric distance between 7 kpc and 9 kpc. Since the age range of our sample does not cover the youngest stars, we also plot the AVR recently obtained by Tarricq et al. 2021 [49] using a sample of 418 Gaia-confirmed OCs (open clusters) in the solar neighbourhood. We note that the AVR at age < 7 Gyr can be well described with a power law [50–53], which is different from the power-law fitting of OC sample. Fig.A7b shows the AVR of local disc stars with a guiding radius between 7 kpc and 9 kpc. Compared with the result based on APOGEE DR17 red giants, we find that our result is more consistent with the result from open clusters [49]. Moreover, the AVR of our sample stars at age < 7 Gyr is in good agreement with those of LAMOST subgiants [16], indicating a good age precision of our sample stars.

A.3 Bayesian linear fits to the radial abundance profiles

In Fig.4 and Fig.A4, we presented the results of Bayesian fits to the radial [Fe/H]/[O/Fe] abundance distributions in age bins of 1 Gyr, using the fitting method described in Anders et al. 2017 [26]. We present the detailed results of these fits for age bins of 1.5-2.5 Gyr in Fig.A8 and Fig.A9.

A.4 The oxygen abundance of young stars from GALAH

To verify that our findings are not caused by artefacts due to selection effects, we plot the Kiel diagram of the stars from the GALAH DR3 in Fig.A10a, color-coded by oxygen abundance. As shown in the Fig.A10, the high temperature MSTO stars with $6200 \text{ K} < T_{\text{eff}} < 7000 \text{ K}$ behave oxygen-enhancement compared with stars at lower temperature end. Most of these oxygen-enhanced stars at high temperature end have ages less than 4 Gyr, which is consistent with our result in Sec.1. Consequently, the oxygen-enhancement in young disc stars in Fig.2 is not due to selection effects, but is directly observed by GALAH survey, and the precise ages of our sample stars allow us to accurately characterize the variation in oxygen abundance of disc stars. In addition, we have examine the oxygen abundance of ~ 15000 common stars from GALAH DR3 and APOGEE DR17, and we did not observe any significant systematic differences in oxygen abundances till 7000 K.

References

- [1] Siegel, M. H. *et al.* The ACS Survey of Galactic Globular Clusters: M54 and Young Populations in the Sagittarius Dwarf Spheroidal Galaxy. *Astrophys. J. Lett.* **667**, L57–L60 (2007).
- [2] Gaia Collaboration *et al.* Gaia Data Release 2. Summary of the contents and survey properties. *Astron. Astrophys.* **616**, A1 (2018).
- [3] Gaia Collaboration *et al.* Gaia Data Release 3. Summary of the content and survey properties. *Astron. Astrophys.* **674**, A1 (2023).

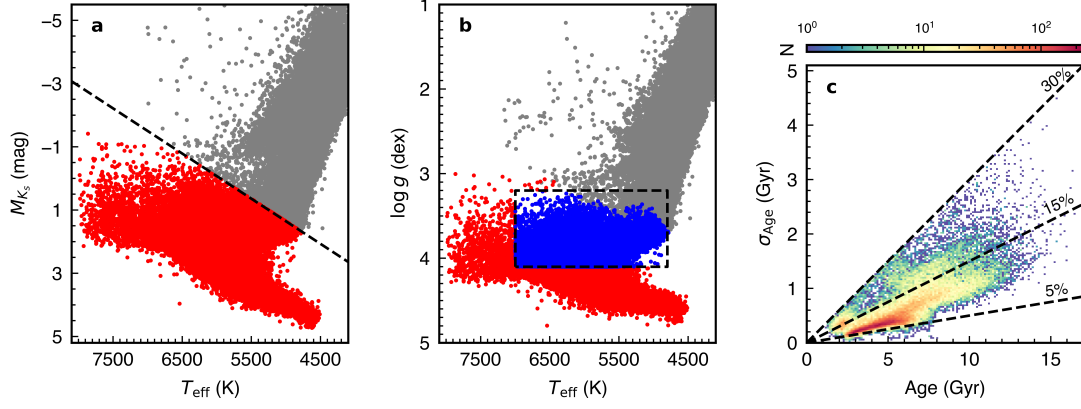


Fig. A1 The MSTO and subgiant star sample with precise ages. **a**, HR diagram of the stars from the GALAH DR3 data (grey dots) and the selected sample (red dots). The black dashed line indicates the cut made to exclude giant stars. **b**, Kiel diagram of the stars from the GALAH DR3 data (grey dots), the selected sample (red dots), and the targets used in our work (blue dots). The MSTO and subgiant stars are delimited by black dashed lines ($3.2 < \log g < 4.1$ and $4800 \text{ K} < T_{\text{eff}} < 7000 \text{ K}$). **c**, Number density distribution in the age uncertainties as a function of age. Black dashed lines represent the 5, 15, and 30 per cent fractional uncertainty levels, respectively.

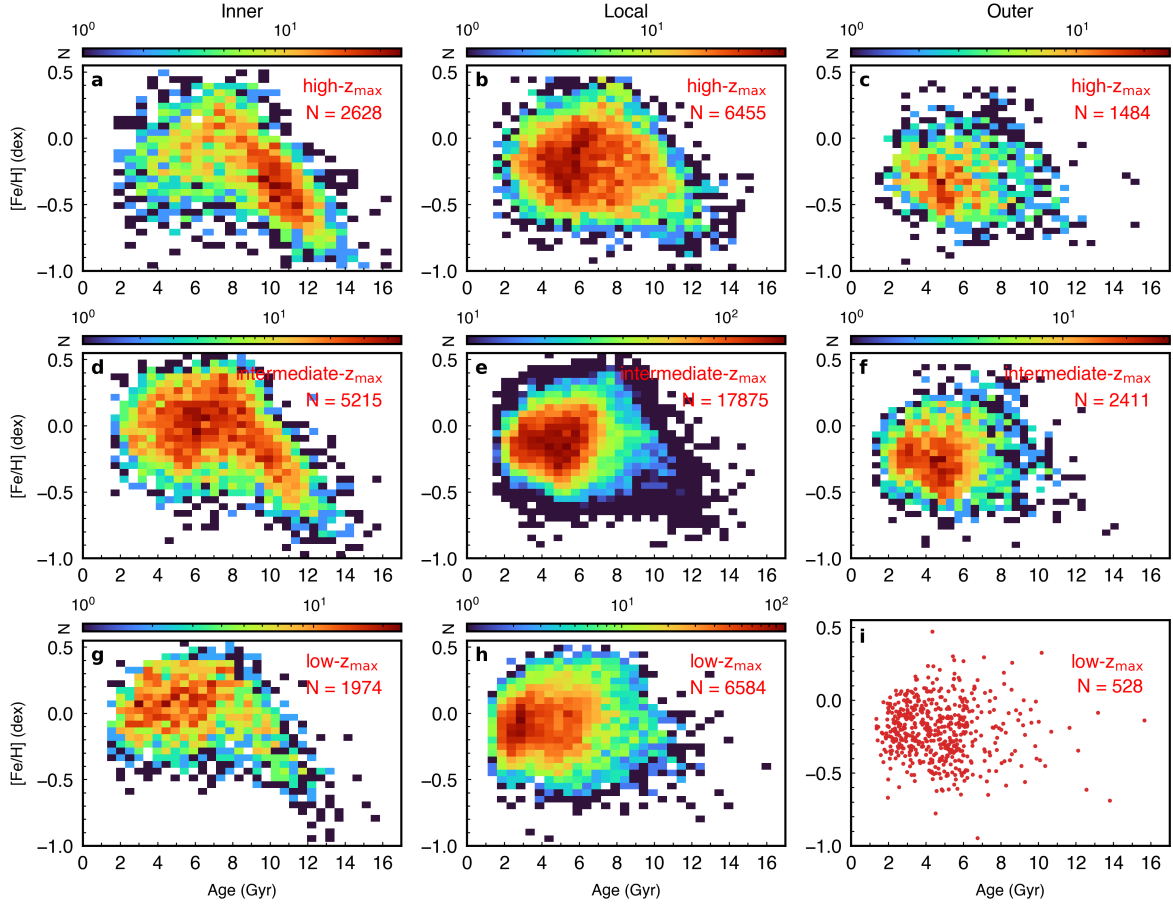


Fig. A2 Age- $[\text{Fe}/\text{H}]$ distributions of the six spatially selected subsamples. **a-i**, arranged according to the division in Figure 1. **a-h**, colour-coded by the stellar number density, N . **i**, red dots represent the stars in outer disc at low- z_{max} region. The numbers of stars in each bin are shown in the top-right corner of each panel.

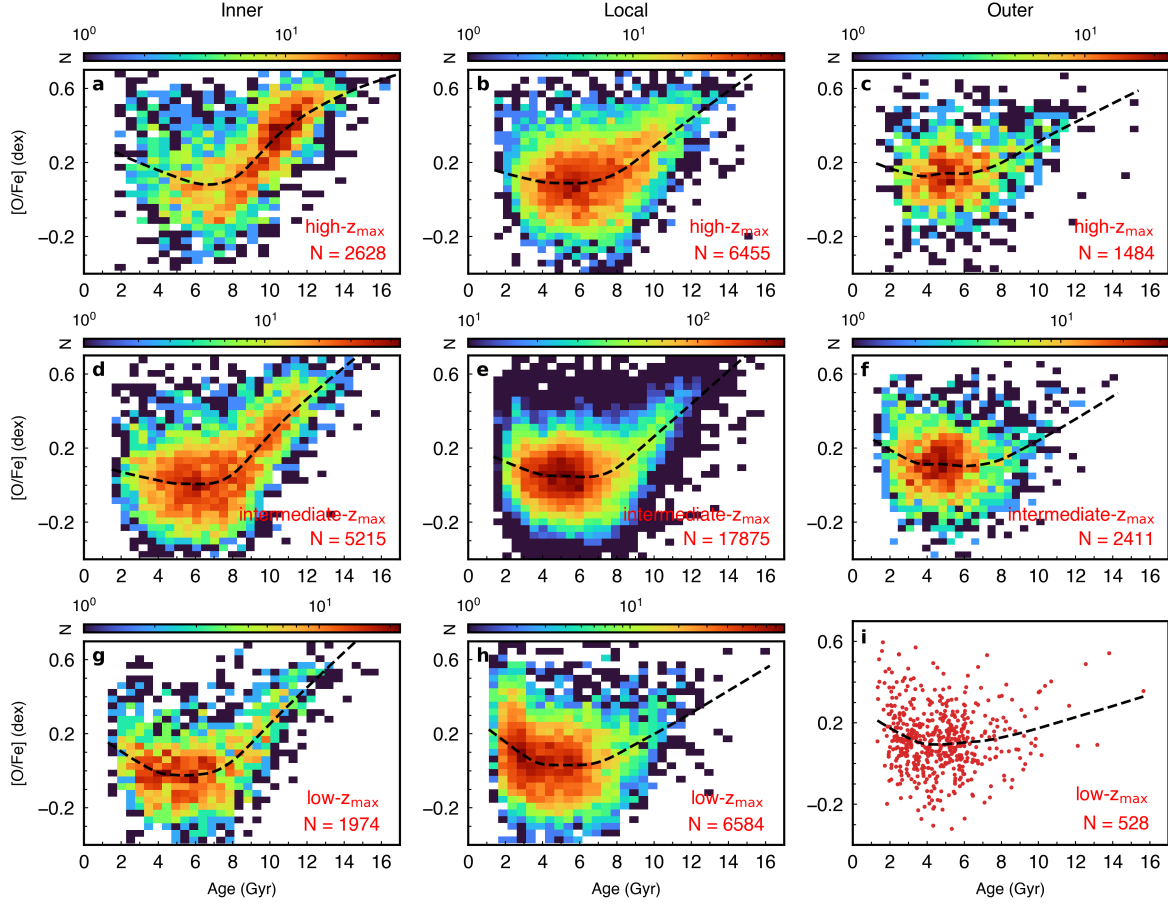


Fig. A3 Age-[O/Fe] distributions of the six spatially selected subsamples. **a-i**, arranged according to the division in Figure 1. **a-h**, colour-coded by the stellar number density, N . **i**, red dots represent the stars in outer disc at low- z_{\max} region. The numbers of stars in each bin are shown in the bottom-right corner of each panel. The black dashed lines represent the fitting result by local nonparametric regression.

- [4] De Silva, G. M. *et al.* The GALAH survey: scientific motivation. *Mon. Not. R. Astron. Soc.* **449**, 2604–2617 (2015).
- [5] Buder, S. *et al.* The GALAH Survey: second data release. *Mon. Not. R. Astron. Soc.* **478**, 4513–4552 (2018).
- [6] Buder, S. *et al.* The GALAH+ survey: Third data release. *Mon. Not. R. Astron. Soc.* **506**, 150–201 (2021).
- [7] Mor, R., Robin, A. C., Figueras, F., Roca-Fàbrega, S. & Luri, X. Gaia DR2 reveals a star formation burst in the disc 2-3 Gyr ago. *Astron. Astrophys.* **624**, L1 (2019).
- [8] Isern, J. The Star Formation History in

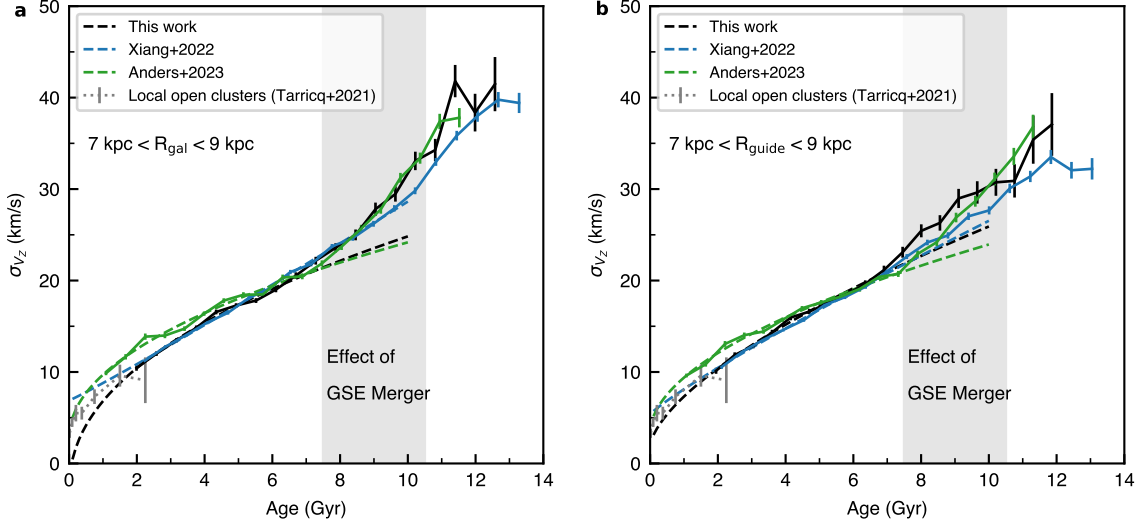


Fig. A4 Comparison of the radial $[\text{Fe}/\text{H}]$ gradient and the corresponding $[\text{Fe}/\text{H}]$ dispersion around the gradient in this work, with the results from LAMOST and APOGEE. **a, b**, The black lines in each panel represent the result of this work, using the GALAH subgiant and MSTO stars; the blue and green lines represent the results from the LAMOST data (LAMOST DR7 subgiant sample [16]) and literature [23] (based on APOGEE DR17 data [30]), respectively.

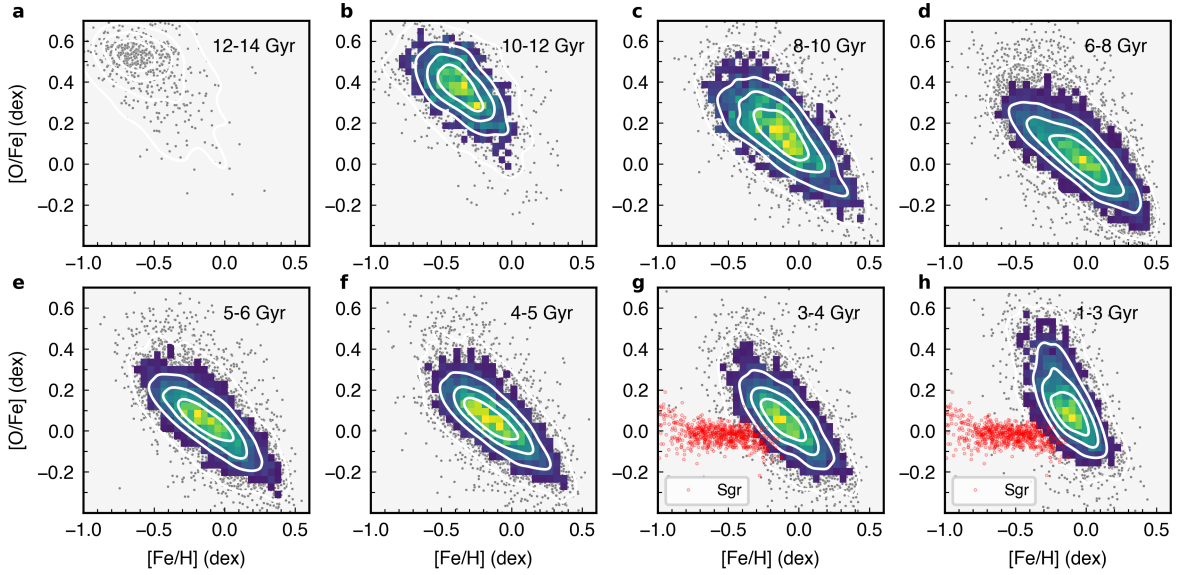


Fig. A5 Distribution of the our sample stars in the $[\text{Fe}/\text{H}]$ - $[\text{O}/\text{Fe}]$ plane at different ages. **a-h**, The contour lines show a kernel density estimation (KDE) with the distribution of the disc stars. The gray dots represent the disc stars in each age bins. The Sgr stars (red dots) are overplotted (**a, h**) for comparison. **b-h**, colour-coded by the stellar number density, N .

the Solar Neighborhood as Told by Massive White Dwarfs. *Astrophys. J. Lett.* **878**, L11 (2019).

[9] Sahlholdt, C. L., Feltzing, S. & Feuillet,

D. K. Characterizing epochs of star formation across the Milky Way disc using age-metallicity distributions of GALAH stars. *Mon. Not. R. Astron. Soc.* **510**, 4669–4688 (2022).

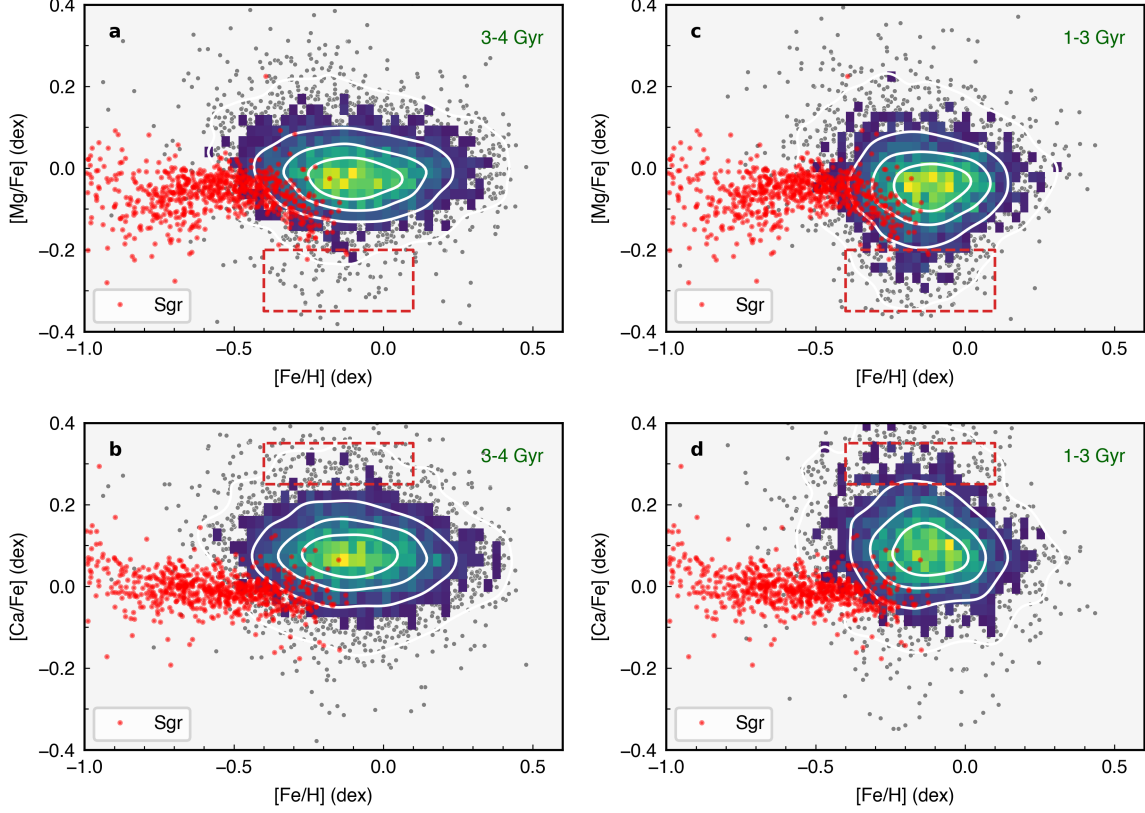


Fig. A6 Distribution of the young stars in the $[\text{Fe}/\text{H}]-[\text{X}/\text{Fe}]$ plane at 1-4 Gyr. **a, b**, Distribution of the stars in the $[\text{Fe}/\text{H}]-[\text{X}/\text{Fe}]$ ($[\text{Mg}/\text{Fe}]$ and $[\text{Ca}/\text{Fe}]$) plane at 3-4 Gyr, and the Sgr stars (red dots) are overplotted for comparison. The red dashed boxes indicate the Mg-poor stars. **c, d**, Similar to **a, b**, but for the younger stars with age between 1-3 Gyr. The red dashed boxes show the Ca-rich stars.

- [10] Sun, T. *et al.* Characterizing abundance-age relations of GALAH stars using oxygen-enhanced stellar models. *Mon. Not. R. Astron. Soc.* **523**, 1199–1208 (2023).
- [11] Tepper-García, T. & Bland-Hawthorn, J. The Sagittarius dwarf galaxy: where did all the gas go? *Mon. Not. R. Astron. Soc.* **478**, 5263–5277 (2018).
- [12] Ruiz-Lara, T., Gallart, C., Bernard, E. J. & Cassisi, S. The recurrent impact of the Sagittarius dwarf on the star formation history of the Milky Way. *Nat. Astron.* **4**, 965–973 (2020).
- [13] Annem, B. & Khoperskov, S. Impact of orbiting satellites on star formation rate evolution and metallicity variations in Milky Way-like discs. *arXiv e-prints* arXiv:2210.17054 (2022).
- [14] Basu, S., Chaplin, W. J. & Elsworth, Y. Determination of Stellar Radii from Asteroseismic Data. *Astrophys. J.* **710**, 1596–1609 (2010).
- [15] Yu, J. *et al.* Revised Extinctions and Radii for 1.5 Million Stars Observed by APOGEE, GALAH, and RAVE. *Astrophys. J. Suppl. Ser.* **264**, 41 (2023).
- [16] Xiang, M. & Rix, H.-W. A time-resolved picture of our Milky Way's early formation history. *Nature* **603**, 599–603 (2022).
- [17] Spitoni, E. *et al.* Beyond the two-infall model. I. Indications for a recent gas infall with Gaia DR3 chemical abundances. *Astron. Astrophys.* **670**, A109 (2023).
- [18] Kobayashi, C., Umeda, H., Nomoto, K., Tomimaga, N. & Ohkubo, T. Galactic Chemical

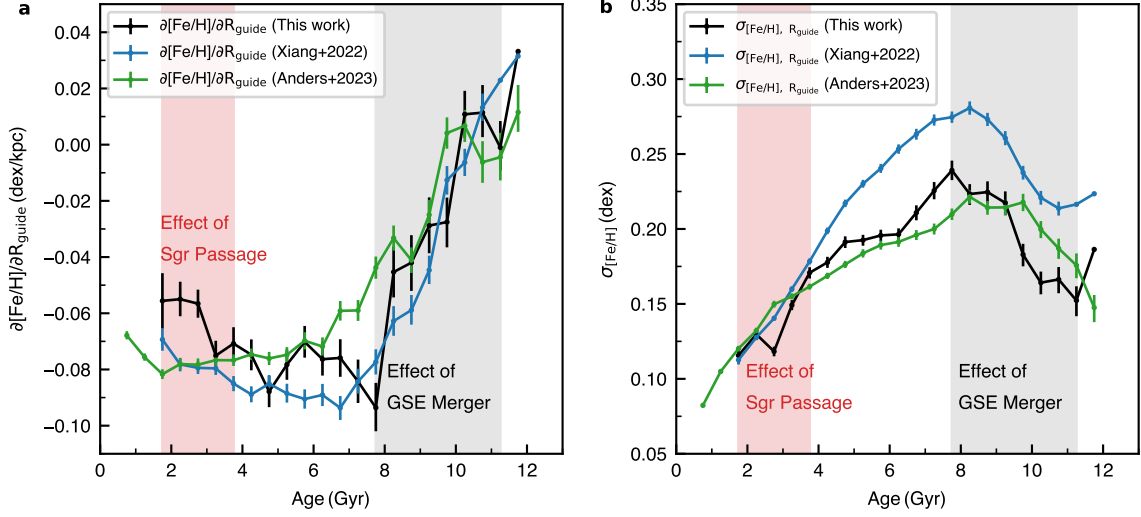


Fig. A7 Age-velocity dispersion relationship of our sample stars in local disc. **a**, Age-velocity dispersion relationship (AVR) of the local disc stars with $7 \text{ kpc} < R_{\text{Gal}} < 9 \text{ kpc}$. The black line represents the result of this work, using the GALAH subgiant and MSTO stars; the blue and green lines represent the results from the LAMOST data (LAMOST DR7 subgiant sample [16]) and APOGEE data [23] (APOGEE DR17 red giant sample [30]), respectively. Also plotted are the results for open clusters in the solar vicinity in literature [49]. The black dashed line corresponds to a simple power-law fit for ages $< 7 \text{ Gyr}$ in the Galactocentric distance bin 7-9 kpc, while the blue and green dashed lines corresponds to the simple power-law fit for the LAMOST subgiants and APOGEE red giants. The shaded region highlights the age range in which we see a steepening in the AVR, potentially related to the GSE merger event. **b**, Similar to **a** but for the local disc stars with $7 \text{ kpc} < R_{\text{guide}} < 9 \text{ kpc}$.

- Evolution: Carbon through Zinc. *Astrophys. J.* **653**, 1145–1171 (2006).
- [19] Kobayashi, C., Karakas, A. I. & Lugaro, M. The Origin of Elements from Carbon to Uranium. *Astrophys. J.* **900**, 179 (2020).
- [20] Sarajedini, A. *et al.* The ACS Survey of Galactic Globular Clusters. I. Overview and Clusters without Previous Hubble Space Telescope Photometry. *Astron. J.* **133**, 1658–1672 (2007).
- [21] Zhao, G. & Chen, Y. Low- α metal-rich stars with sausage kinematics in the LAMOST survey: Are they from the Gaia-Sausage-Enceladus galaxy? *Science China Physics, Mechanics, and Astronomy* **64**, 239562 (2021).
- [22] Lu, Y. *et al.* There is No Place Like Home – Finding Birth Radii of Stars in the Milky Way. *arXiv e-prints* arXiv:2212.04515 (2022).
- [23] Anders, F. *et al.* Spectroscopic age estimates for 180 000 APOGEE red-giant stars: Precise spatial and kinematic trends with age in the Galactic disc. *arXiv e-prints* arXiv:2304.08276 (2023).
- [24] Ratcliffe, B. *et al.* Unveiling the time evolution of chemical abundances across the Milky Way disk with APOGEE. *Mon. Not. R. Astron. Soc.* (2023).
- [25] Lian, J., Bergemann, M., Pillepich, A., Zasowski, G. & Lane, R. R. The integrated metallicity profile of the Milky Way. *Nat. Astron.* 2397–3366 (2023).
- [26] Anders, F. *et al.* Red giants observed by CoRoT and APOGEE: The evolution of the Milky Way’s radial metallicity gradient. *Astron. Astrophys.* **600**, A70 (2017).
- [27] Cui, X.-Q. *et al.* The Large Sky Area Multi-Object Fiber Spectroscopic Telescope (LAMOST). *Res. Astron. Astrophys.* **12**, 1197–1242

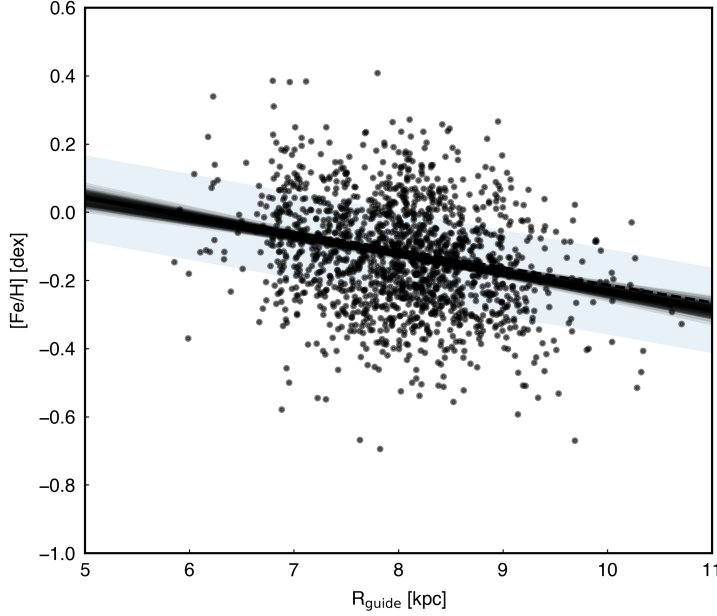


Fig. A8 Examples of the fits to the $[\text{Fe}/\text{H}]$ vs. R_{guide} distributions for age bins of 1.5-2.5 Gyr. The black dots represent the distribution of the sample stars in this age bin. The thick black line shows the result of a naive least-squares linear fit. The thin grey lines show 30 realisations drawn from the linear gradient + intrinsic scatter posterior, while the shaded band corresponds the 1σ dispersion around the gradient.

(2012).

(2013).

- [28] Zhao, G., Zhao, Y.-H., Chu, Y.-Q., Jing, Y.-P. & Deng, L.-C. LAMOST spectral survey — An overview. *Res. Astron. Astrophys.* **12**, 723–734 (2012).
- [29] Majewski, S. R. *et al.* The Apache Point Observatory Galactic Evolution Experiment (APOGEE). *Astron. J.* **154**, 94 (2017).
- [30] Abdurro’uf *et al.* The Seventeenth Data Release of the Sloan Digital Sky Surveys: Complete Release of MaNGA, MaStar, and APOGEE-2 Data. *Astrophys. J. Suppl. Ser.* **259**, 35 (2022).
- [31] Law, D. R. & Majewski, S. R. The Sagittarius Dwarf Galaxy: A Model for Evolution in a Triaxial Milky Way Halo. *Astrophys. J.* **714**, 229–254 (2010).
- [32] McWilliam, A., Wallerstein, G. & Mottini, M. Chemistry of the Sagittarius Dwarf Galaxy: A Top-light Initial Mass Function, Outflows, and the R-process. *Astrophys. J.* **778**, 149 (2013).
- [33] Hasselquist, S. *et al.* APOGEE Chemical Abundances of the Sagittarius Dwarf Galaxy. *Astrophys. J.* **845**, 162 (2017).
- [34] Mucciarelli, A. *et al.* Chemical abundances in the nucleus of the Sagittarius dwarf spheroidal galaxy. *Astron. Astrophys.* **605**, A46 (2017).
- [35] Hasselquist, S. *et al.* Identifying Sagittarius Stream Stars by Their APOGEE Chemical Abundance Signatures. *Astrophys. J.* **872**, 58 (2019).
- [36] Hayes, C. R. *et al.* Metallicity and α -Element Abundance Gradients along the Sagittarius Stream as Seen by APOGEE. *Astrophys. J.* **889**, 63 (2020).
- [37] Hasselquist, S. *et al.* APOGEE Chemical Abundance Patterns of the Massive Milky Way Satellites. *Astrophys. J.* **923**, 172 (2021).

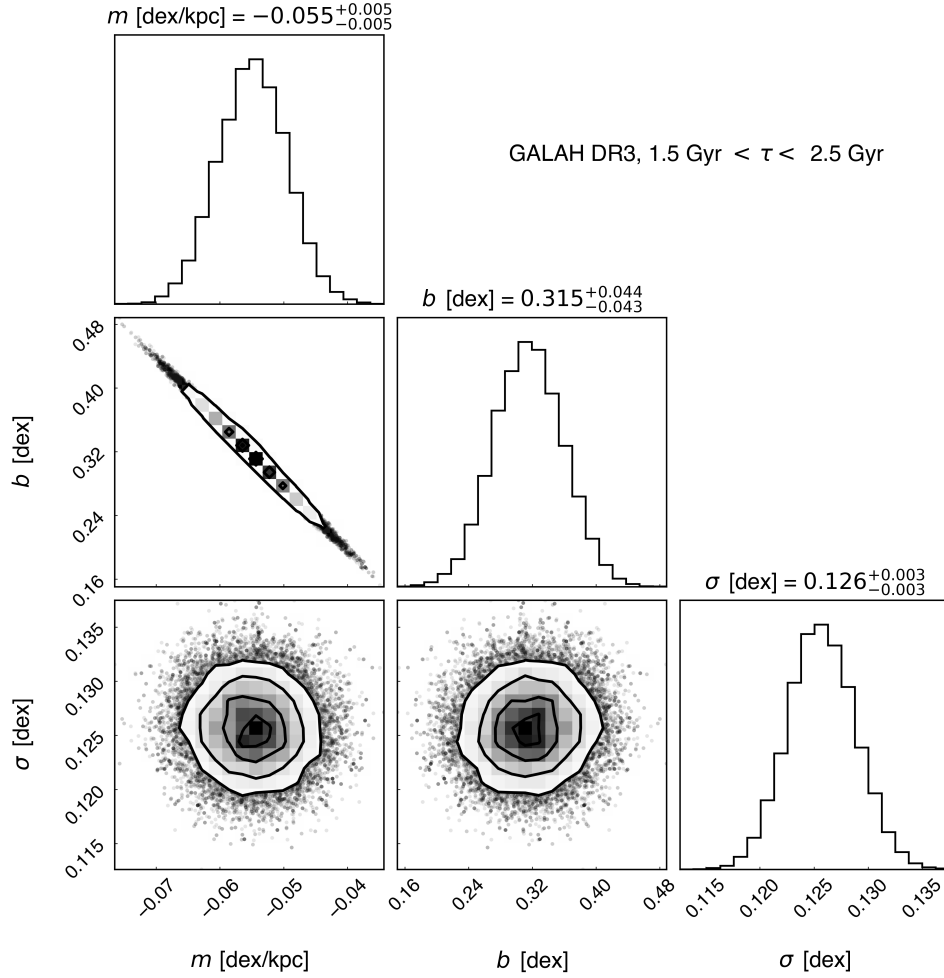


Fig. A9 Posterior distributions of the fit parameters ($m = \partial[\text{Fe}/\text{H}]/\partial R$, b (intercept at $R = 0$), and σ (intrinsic $[\text{Fe}/\text{H}]$ dispersion).

- [38] Fernandes, L. *et al.* A comparative analysis of the chemical compositions of Gaia-Enceladus/Sausage and Milky Way satellites using APOGEE. *Mon. Not. R. Astron. Soc.* **519**, 3611–3622 (2023).
- [39] Magrini, L. *et al.* The Gaia-ESO Survey: radial distribution of abundances in the Galactic disc from open clusters and young-field stars. *Astron. Astrophys.* **603**, A2 (2017).
- [40] Franchini, M. *et al.* The Gaia-ESO Survey: Oxygen Abundance in the Galactic Thin and Thick Disks. *Astron. J.* **161**, 9 (2021).
- [41] Amarsi, A. M. *et al.* The GALAH Survey: non-LTE departure coefficients for large spectroscopic surveys. *Astron. Astrophys.* **642**, A62 (2020).
- [42] Traven, G. *et al.* The GALAH survey: multiple stars and our Galaxy. I. A comprehensive method for deriving properties of FGK binary stars. *Astron. Astrophys.* **638**, A145 (2020).
- [43] Skrutskie, M. F. *et al.* The Two Micron All Sky Survey (2MASS). *Astron. J.* **131**, 1163–1183 (2006).
- [44] Planck Collaboration *et al.* Planck 2015 results. XIII. Cosmological parameters.

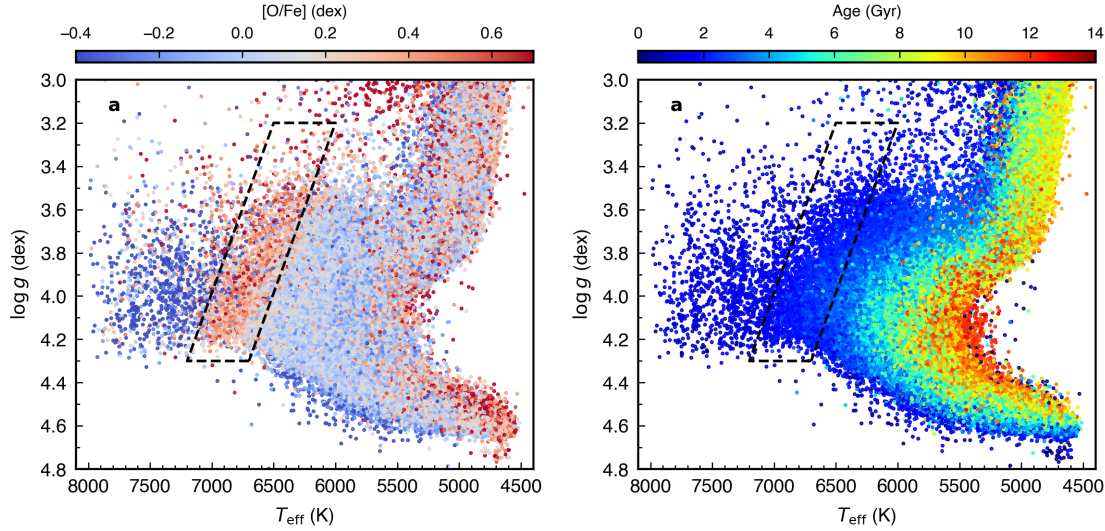


Fig. A10 The oxygen abundance of GALAH stars. **a**, Kiel diagram of the stars from the GALAH DR3 data, colour-coded by oxygen abundance. **b**, Kiel diagram of the stars from the GALAH DR3 data, colour-coded by ages from GALAH value-added catalogue [6]. The black dashed boxes indicate the young O-rich stars.

Astron. Astrophys. **594**, A13 (2016).

- [45] Gaia Collaboration *et al.* Gaia Data Release 3. Chemical cartography of the Milky Way. *Astron. Astrophys.* **674**, A38 (2023).

- [46] Zwitter, T. *et al.* The GALAH+ survey: a new library of observed stellar spectra improves radial velocities and hints at motions within M67. *Mon. Not. R. Astron. Soc.* **508**, 4202–4215 (2021).

- [47] Bovy, J. galpy: A python Library for Galactic Dynamics. *Astrophys. J. Suppl. Ser.* **216**, 29 (2015).

- [48] Sun, T. *et al.* Age of FGK Dwarfs Observed with LAMOST and GALAH: Considering the Oxygen Enhancement. *Astrophys. J. Suppl. Ser.* **268**, 29 (2023).

- [49] Tarricq, Y. *et al.* 3D kinematics and age distribution of the open cluster population. *Astron. Astrophys.* **647**, A19 (2021).

- [50] Aumer, M., Binney, J. & Schönrich, R. Age-velocity dispersion relations and heating histories in disc galaxies. *Mon. Not. R. Astron. Soc.* **462**, 1697–1713 (2016).

- [51] Yu, J. & Liu, C. The age-velocity dispersion

relation of the Galactic discs from LAMOST-Gaia data. *Mon. Not. R. Astron. Soc.* **475**, 1093–1103 (2018).

- [52] Ting, Y.-S. & Rix, H.-W. The Vertical Motion History of Disk Stars throughout the Galaxy. *Astrophys. J.* **878**, 21 (2019).

- [53] Agertz, O. *et al.* VINTERGATAN - I. The origins of chemically, kinematically, and structurally distinct discs in a simulated Milky Way-mass galaxy. *Mon. Not. R. Astron. Soc.* **503**, 5826–5845 (2021).